










Review

Direct and Indirect Measurements of the $^{19}\text{F}(p,\alpha)^{16}\text{O}$ Reaction at Astrophysical Energies Using the LHASA Detector and the Trojan Horse Method

Giovanni L. Guardo ¹, Giuseppe G. Rapisarda ^{1,2,*}, Dimiter L. Balabanski ^{3,4}, Giuseppe D'Agata ², Alessia Di Pietro ¹, Pierpaolo Figuera ¹, Marco La Cognata ¹, Marco La Commara ^{5,6}, Livio Lamia ^{1,2,7}, Dario Lattuada ^{1,8}, Catalin Matei ³, Marco Mazzocco ^{9,10}, Alessandro A. Oliva ¹, Sara Palmerini ^{11,12}, Teodora Petrusse ^{3,4}, Rosario G. Pizzone ^{1,2}, Stefano Romano ^{1,2,7}, Maria Letizia Sergi ^{1,2}, Roberta Spartá ^{1,8}, Xuedou Su ^{9,13}, Aurora Tumino ^{1,8} and Nikola Vukman ^{12,14}

- ¹ INFN-Laboratori Nazionali del Sud, 95123 Catania, Italy; guardo@lns.infn.it (G.L.G.)
 - ² Dipartimento di Fisica e Astronomia 'Ettore Majorana', Università di Catania, 95123 Catania, Italy
 - ³ Extreme Light Infrastructure Nuclear Physics/IFIN-HH, 077125 Magurele, Romania
 - ⁴ Scoala Doctorala de Ingineria si Aplicatiile Laserilor si Acceleratorilor, Universitatea Politehnica, 060042 Bucuresti, Romania
 - ⁵ Dipartimento di Farmacia, Università di Napoli 'Federico II', 80131 Napoli, Italy
 - ⁶ INFN-Sezione di Napoli, 80126 Napoli, Italy
 - ⁷ Centro Siciliano di Fisica Nucleare e Struttura della Materia (CSFNSM), 95123 Catania, Italy
 - ⁸ Dipartimento di Ingegneria e Architettura, Università degli Studi di Enna 'Kore', 94100 Enna, Italy
 - ⁹ Dipartimento di Fisica e Astronomia 'Galileo Galilei', Università di Padova, 35121 Padova, Italy
 - ¹⁰ INFN-Sezione di Padova, 35121 Padova, Italy
 - ¹¹ Dipartimento di Fisica e Geologia, Università degli Studi di Perugia, 06123 Perugia, Italy
 - ¹² INFN-Sezione di Perugia, 06123 Perugia, Italy
 - ¹³ School of Physics, Beihang University, Beijing 100191, China
 - ¹⁴ Rudjer Boskovic Institute, 10000 Zagreb, Croatia
- * Correspondence: giuseppe.rapisarda@unict.it



Citation: Guardo, G.L.; Rapisarda, G.G.; Balabanski, D.L.; D'Agata, G.; Di Pietro, A.; Figuera, P.; La Cognata, M.; La Commara, M.; Lamia, L.; Lattuada, D.; et al. Direct and Indirect Measurements of the $^{19}\text{F}(p,\alpha)^{16}\text{O}$ Reaction at Astrophysical Energies Using the LHASA Detector and the Trojan Horse Method. *Universe* **2024**, *10*, 304. <https://doi.org/10.3390/universe10070304>

Academic Editor: Andreas Aste

Received: 6 June 2024

Revised: 8 July 2024

Accepted: 15 July 2024

Published: 22 July 2024



Copyright: © 2024 by the authors. Licensee MDPI, Basel, Switzerland. This article is an open access article distributed under the terms and conditions of the Creative Commons Attribution (CC BY) license (<https://creativecommons.org/licenses/by/4.0/>).

Abstract: Fluorine is one of the most interesting elements in nuclear astrophysics. Its abundance can provide important hints to constrain the stellar models since fluorine production and destruction are strictly connected to the physical conditions inside the stars. The $^{19}\text{F}(p,\alpha)^{16}\text{O}$ reaction is one of the fluorine burning processes and the correction evaluation of its reaction rate is of pivotal importance to evaluate the fluorine abundance. Moreover, the $^{19}\text{F}(p,\alpha)^{16}\text{O}$ reaction rate can have an impact for the production of calcium in the first-generation of Population III stars. Here, we present the AsFiN collaboration efforts to the study of the $^{19}\text{F}(p,\alpha)^{16}\text{O}$ reaction by means of direct and indirect measurements. On the direct measurements side, an experimental campaign aimed to the measurement of the $^{19}\text{F}(p,\alpha_0,\pi)^{16}\text{O}$ reaction is ongoing, taking advantage of the new versatile arrays of silicon strip detectors, LHASA and ELISSA. Moreover, the Trojan Horse Method (THM) was used to determine the $^{19}\text{F}(p,\alpha_0)^{16}\text{O}$ reaction $S(E)$ -factor in the energy range of astrophysical interest ($E_{cm} \approx 0\text{--}1$ MeV), showing, for the first time, the presence of resonant structures within the astrophysical energy range. THM has been also applied for the study of the $^{19}\text{F}(p,\alpha_\pi)^{16}\text{O}$ reaction; data analysis is ongoing.

Keywords: nuclear reaction; nuclear astrophysics; nucleosynthesis; reaction rate; AGB stars; silicon array; indirect measurement

1. Introduction

Fluorine production occurs in the He-rich intershell region of Asymptotic Giant Branch (AGB) stars, coinciding with the region where s-process elements are synthesized. Consequently, fluorine is transported to the stellar surface alongside s-process elements during convective dredge-up episodes. This makes the abundance of fluorine a valuable diagnostic

tool for understanding AGB stellar models and nucleosynthesis processes, particularly aiding in the analysis of *s*-process mechanisms under AGB star conditions. Hence, comprehending the synthesis of fluorine is crucial for advancing our understanding of *s*-process nucleosynthesis in AGB stars [1,2].

The issue lies in the deficiency of current models to account for the F overabundance observed in low-mass AGB stars [3]. A potential solution could emerge from a reassessment of the nuclear reaction rates governing the production and depletion of this element within these stellar environments. One of the main processes responsible for the fluorine destruction is the $^{19}\text{F}(p,\alpha)^{16}\text{O}$ reaction, which takes place in the H-burning shell [4]. A recent study was conducted by Palmerini et al. [5] considering extra mixing within the AGB stars and the new evaluation of the $^{19}\text{F}(p,\alpha)^{16}\text{O}$ reaction rate [6,7]. Their findings revealed a reduction of about 50% in the surface abundance of ^{19}F , with respect to calculations performed considering reaction rates reported in the Nuclear Astrophysics Compilation of Reaction Rates (NACRE) [8]. In the H-burning shell, fluorine is also burned by the $^{19}\text{F}(p,\gamma)^{20}\text{Ne}$ reaction, which has been considered up to now less efficient compared to the (p,α) channel. A recent paper pointed out that the $(p,\gamma)/(p,\alpha)$ ratio of about a factor ten times higher than that reported in the NACRE compilation [8] could explain the abundance of ^{40}Ca observed in ultra-metal-poor stars such as SMSS0313-6708 [9]. Indeed, a breakout from the CNO cycles, characterized by the leakage from the CNO cycle to the NeNa cycle via the $^{19}\text{F}(p,\gamma)^{20}\text{Ne}$ reaction, is influenced not only by the abundance of ^{19}F but also by the reaction rates of the $^{19}\text{F}(p,\gamma)^{20}\text{Ne}$ reaction and the competing $^{19}\text{F}(p,\alpha)^{16}\text{O}$ reaction [10,11]. This theoretical calculation has been corroborated by the measurement performed by [11] where the $^{19}\text{F}(p,\gamma)^{20}\text{Ne}$ reaction rate showed an important increase in the $(p,\gamma)/(p,\alpha)$ ratio with respect to the NACRE recommended one. It is worth noting that the NACRE reaction rate for the (p,α) reaction channel was obtained extrapolating only a non-resonant contribution at low energies of astrophysical interest.

Although crucial, the astrophysical $S(E)$ -factor remains significantly uncertain at astrophysical energies [12], emphasizing the necessity for improved measurements. In particular, the $^{19}\text{F}(p,\alpha)^{16}\text{O}$ reaction rate is the sum of the rates related to the three open channels, namely (p,α_0) , (p,α_π) and (p,α_γ) , where the ^{16}O is left in its ground state, first excited state (6049.4 keV, 0^+) and second excited state (6129.89 keV, 3^-), respectively. In addition, from close examination of the data available in the literature, it can be asserted that taking into account only the (p,α_0) channel, as mentioned in [3,13,14], until a few years ago, the only data present in the studies [15–18] in the $E_{c.m.} = 0.46\text{--}2.54$ MeV energy domain were the extrapolated $S(E)$ -factor values reported in NACRE [8], while almost nothing was known from experiments on the (p,α_π) and (p,α_γ) rates at very low energies.

In the last years, some experimental efforts were made to improve the situation, especially for the (p,α_0) [19] and (p,α_γ) [10] channels. In this review, we will describe the contribution of the AsFiN collaboration to the study of the $^{19}\text{F}(p,\alpha)^{16}\text{O}$ reaction by means of direct and indirect measurements.

2. Direct Approach: The LHASA Detector

As mentioned, a direct measurement of the $^{19}\text{F}(p,\alpha_0)^{16}\text{O}$ reaction was recently carried out in the energy range $E_{c.m.} = 0.2\text{--}1$ MeV [19,20]. In the energy region $E_{c.m.} > 0.8$ MeV, the new results are consistent with the data in the NACRE compilation. However, for energies below 0.8 MeV, the data from [19] align with those from [15], yet they are approximately 1.4 times higher than the data reported by [16], as illustrated in Figure 1. Due to this large discrepancy with respect to the previous data, in correspondence of the peaks centred at 681 and 738 keV in the centre of mass system, a new direct measurement was planned to focus on the energy range of $E_{c.m.} = 400\text{--}900$ keV, and to derive the astrophysical $S(E)$ -factor with the aim of resolving the discrepancies that exist between the previously available data sets in the literature.

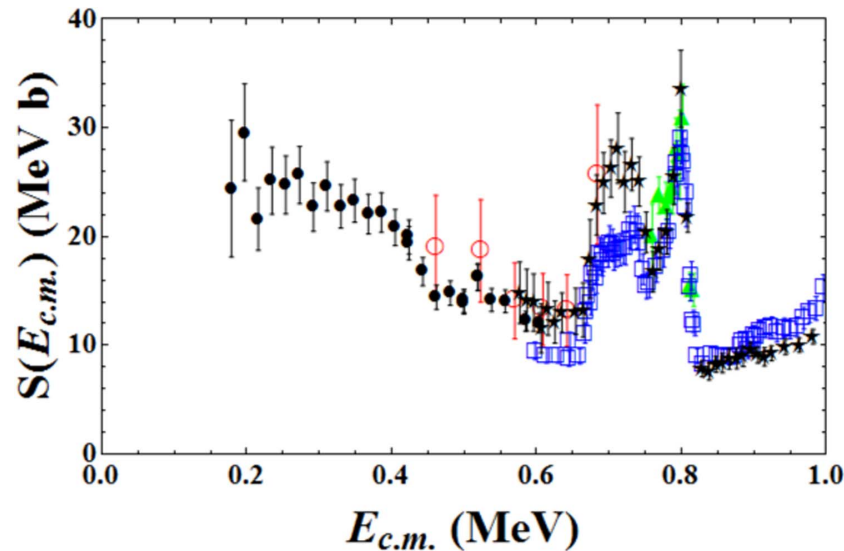


Figure 1. Available direct data for the $^{19}\text{F}(p,\alpha_0)^{16}\text{O}$ reaction. The empty red circles show the data of [15], the empty blue squares the data of [16], the green triangles the data of [17], the black stars the data of [20] and the black circles the data of [19].

The experiment was conducted at INFN—Laboratori Nazionali del Sud in Catania, Italy. The 15 MV Van de Graaf Tandem accelerator provided a ^{19}F beam with energies ranging from 9 to 18.5 MeV, a spot size of 1 mm on the target, and intensities of approximately 1–5 nA. Thin self-supported polyethylene (CH_2) targets, about $100\ \mu\text{g}/\text{cm}^2$ in thickness, were positioned at 90° to the beam direction and were frequently replaced to prevent degradation.

The detection setup, reported in the Figure 2, consisted of 6 YY1 silicon strip detectors with a thickness of $300\ \mu\text{m}$ [21]. The detectors were mounted in a lamp-shade configuration forming an array called LHASA (Large High-resolution Array of Silicon for Astrophysics) [22]. LHASA was optimized to detect emerging alpha particles over a wide angular range (from 10° to 32°) and positioned 10 cm from the target. To suppress significant fluorine and carbon scattering, a thin aluminum shield ($15\ \mu\text{m}$ thick) was placed in front of the LHASA detector. This setup introduced a 4 MeV threshold for α -particle detection and an overall energy straggling of approximately 40 keV. However, this did not pose a problem for the experiment, as kinematic calculations indicated that alpha particles from the $^1\text{H}+^{19}\text{F}$ interaction would have a minimum energy of 7 MeV.

Energy calibration was performed by means of ^6Li elastic and inelastic scattering in the 12–20 MeV energy range through the interaction with Au and C target and by using a ^{228}Th α -source. The calibration was checked with an open-source Monte Carlo simulation, made fully independent of the data, based on GEANT4 tracking libraries and the n-body event generator called GROOT [23] within the ROOT framework [24]. The result shows excellent agreement and demonstrates the quality of the calibrations, as reported in Figure 3 where the black dots represent the simulated points superimposed on the experimental data at 18.5 MeV.

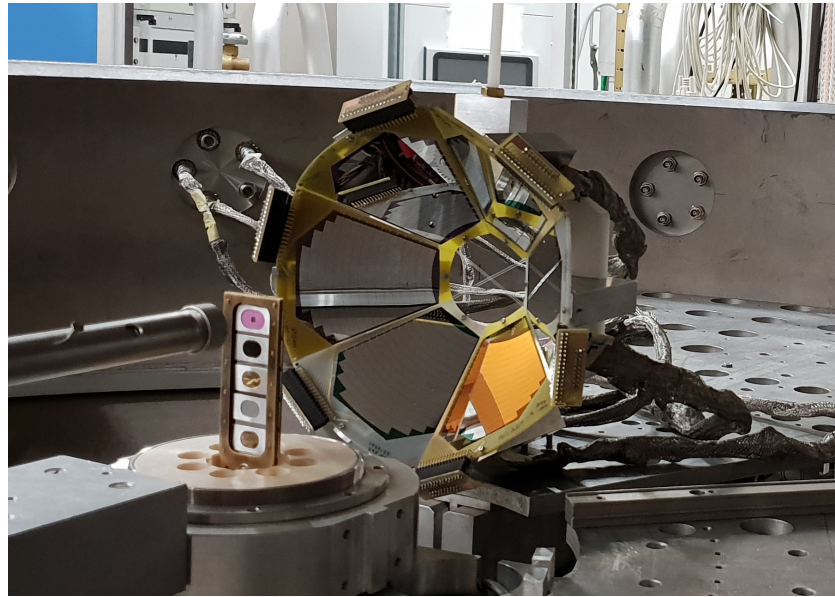


Figure 2. Picture of the detector LHASA used for the experiment.

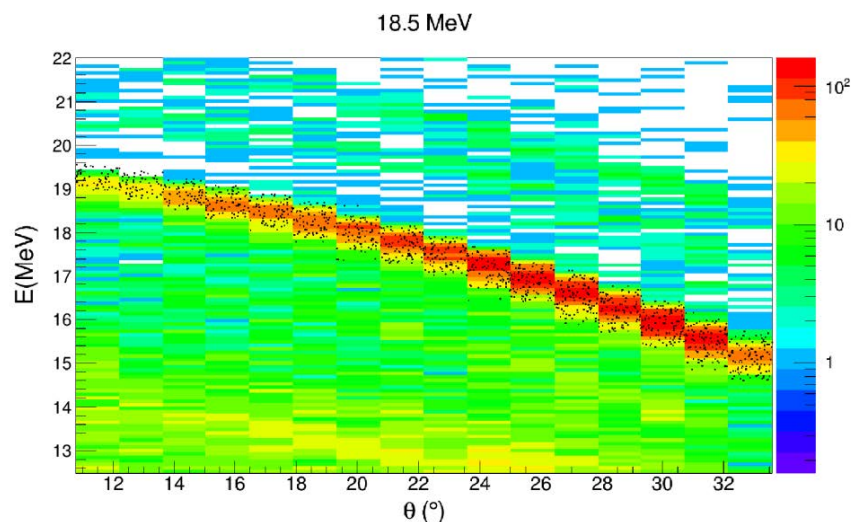


Figure 3. Comparison between experimental data (coloured points) and simulated one (black points) for the beam energy of 18.5 MeV (see text for details).

For extracting the cross-section, it is needed to determine the number of particles in the beam, the number of particles in the target and the number of interactions. The first two parameters were measured by means of a Faraday cup placed behind the target and a monitor detector placed at 45° with respect to the beam axis, at a distance of 70 cm from the target. Integrating over the number of reactions in each strip of the LHASA detection array, the angular distribution for the $^{19}\text{F}(p,\alpha_0)^{16}\text{O}$ reaction is determined. One example of such procedure is presented in Figure 4. In the angular distribution for 725 keV in the center-of-mass system, the experimental points (blue symbols) are overlapped with a sum of the first 5-order Legendre polynomials (red line). The number of reactions was determined by integrating over the scaled sum of Legendre polynomials. Having all quantities, the $^{19}\text{F}(p,\alpha_0)^{16}\text{O}$ cross-section together with the astrophysical $S(E)$ -factor are calculated. A detailed description of the experimental setup and data analysis can be found in [25,26].

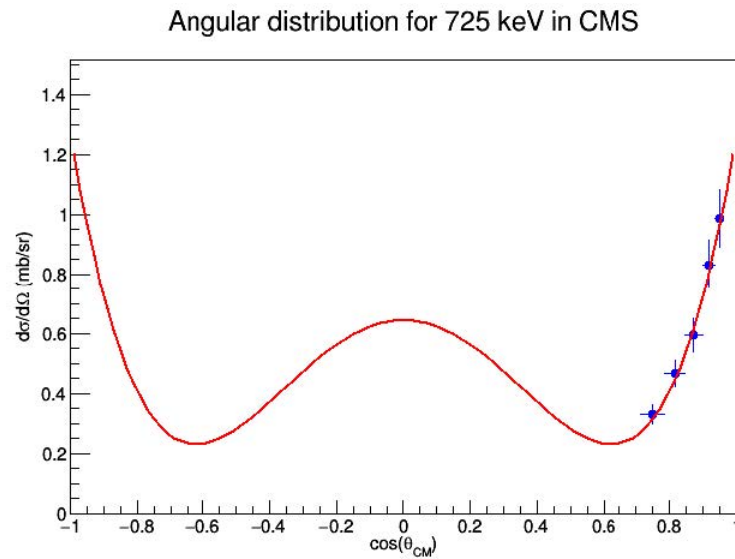


Figure 4. Angular distribution for 725 keV in the center-of-mass system. The experimental points (blue symbols) are overlapped with a sum of the first 5-order Legendre polynomials (red line).

3. Indirect Approach: Trojan Horse Method

The study of the $^{19}\text{F}(p,\alpha)^{16}\text{O}$ has also been tackled using the experimental indirect Trojan Horse Method (THM) (see [27–29] for recent reviews). This well-established indirect technique allows for the measurement of nuclear reactions relevant for astrophysics down to the sub-Coulomb low-energy region typical of astrophysical environments. By selecting the quasi-free (QF) contribution from the reaction yield of a suitable $2 \rightarrow 3$ body reaction $a + A \rightarrow c + C + s$, THM allows to determine the cross-section of a two-body process $x + A \rightarrow c + C$, at astrophysical energies devoid of Coulomb and centrifugal barrier suppression, as well as electron screening effects. The Trojan Horse (TH) nucleus a is selected to have a high probability for a cluster configuration $x \oplus s$. The three-body reaction is induced at energies higher than the Coulomb barrier, in order to induce the break-up of a inside the nuclear field. Then, the transferred particles x induces the two-body process of astrophysical interest, while s is *spectator* to the two-body process. Despite the high value of the beam energy, the $x + A \rightarrow c + C$ reaction is induced at the low energies of interest, thanks to the effect of the TH nucleus binding energy.

The Trojan Horse reaction is usually described in plane wave impulse approximation (PWIA) formalism, where the three-body cross-section is factorized as in the following equation:

$$\frac{d^3\sigma}{dE_c d\Omega_c d\Omega_C} \propto \text{KF} \cdot |\Phi(\vec{p}_{xs})|^2 \cdot \left. \frac{d\sigma}{d\Omega} \right|_{c.m.}^{\text{HOES}} \quad (1)$$

where KF is the kinematical factor, $|\Phi(\vec{p}_{xs})|^2$ is the squared modulus of the Fourier transform of the radial wave function describing the $x - s$ relative motion. $d\sigma/d\Omega|_{c.m.}^{\text{HOES}}$ is the half-off-energy-shell (HOES) differential cross-section for the $A(x, c)C$ process.

The center of mass energy of the two-body process is calculated in post-collision prescription as $E_{c.m.} = E_{cC} - Q$, where Q is the Q-value of the $A(x, c)C$ reaction and E_{cC} is the relative $c - C$ energy. The two-body cross-section is HOES since the transferred particle x is *virtual* and the mass-shell equation is not satisfied, that is, $E_x \neq k_x^2/(2m_x)$ [30].

For multiresonant reactions, as for the $^{19}\text{F}(p,\alpha)^{16}\text{O}$ case, the modified R-matrix approach of [6,31] has been developed. Assuming that the two-body reaction $A(x, c)C$ occurs

via isolated non-interfering resonances, the cross-section that describes the binary process is given in PWIA by the following equation:

$$\frac{d^2\sigma}{dE_{xA}d\Omega_s} = NF \sum_i (2J_i + 1) \times \left| \sqrt{\frac{k_f(E_{xA})}{\mu_{cC}}} \frac{\sqrt{2P_{l_i}(k_{cC}R_{cC})} M_i(p_{xA}R_{xA}) \gamma_{cC}^i \gamma_{xA}^i}{D_i(E_{xA})} \right|^2 \quad (2)$$

where NF is a normalization factor, J_i is the spin of the i -th resonance, $k_f(E_{xA}) = \sqrt{2\mu_{cC}(E_{xA} + Q)}/\hbar$ (Q is the reaction Q -value, E_{xA} the $x - A$ relative energy), P_{l_i} the penetration factor in l_i -wave, R_{xA} and R_{cC} the channel radii. $M_i(p_{xA}R_{xA})$ is the amplitude of the transfer reaction which replaces the square root of the penetration factor in the entry channel, $D_i(E_{xA})$ is the standard R-matrix denominator for the one-level multi-channel case. γ_{cC}^i and γ_{xA}^i are the reduced widths for the i -th resonance and are the same that appear in the standard R-matrix calculation. By fitting the experimental THM cross-section, the reduced widths of the measured resonances can be obtained and used to deduce the $A(x, c)C$ cross-section. Normalization is achieved by extending the indirect measurement to higher energies where direct measurement are available together with the resonances parameters. Over the past few decades, THM has been utilized extensively in the investigation of charged-particle reactions, along with neutron-induced reactions, which play crucial roles in various astrophysical scenarios (see [32–42] for recent results and reviews).

3.1. $^{19}\text{F}(p,\alpha)^{16}\text{O}$ via THM

The $^{19}\text{F}(p,\alpha)^{16}\text{O}$ reaction has been studied applying the THM to the three-body reaction $^2\text{H}(^{19}\text{F},\alpha\ ^{16}\text{O})\text{n}$ where the deuteron was selected as the TH nucleus for the $(p \oplus n)$ configuration. As described by the diagram in Figure 5 the ^{19}F -d interaction induces the deuteron break-up allowing the transfer of the proton that interacts with the ^{19}F to induce the two-body process while the neutron *spectator* does not interfere with the two-body process.

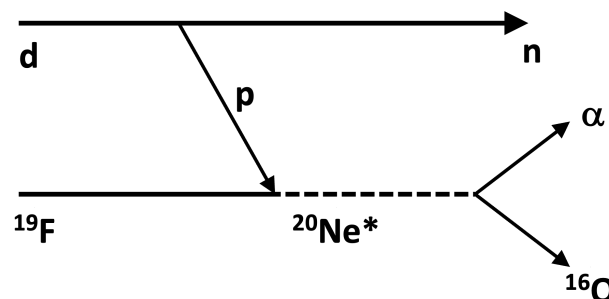


Figure 5. Scheme of the TH reaction $^2\text{H}(^{19}\text{F},\alpha\ ^{16}\text{O})\text{n}$ in QF kinematics.

3.1.1. Experimental Setup

The THM measurements have been dedicated to the study of the $^{19}\text{F}(p,\alpha_0)^{16}\text{O}$ channel with the emitted ^{16}O in the ground state. Two experiments were performed. The first experiment was carried out at LNS-INFN, Catania where a 50 MeV ^{19}F beam was delivered onto a CD_2 target ($\sim 100 \mu\text{g cm}^{-2}$) [6]. In order to improve the experimental resolution, the second experiment performed at INFN-LNL, Legnaro with a 55 MeV ^{19}F beam was delivered onto a CD_2 target ($95 \mu\text{g cm}^{-2}$) [7]. Beam energies were selected in order to overcome the Coulomb barrier of the entrance channel.

The experimental setup and data analysis procedure were quite similar for the two experimental runs. In what follows, explicit reference will be made to the second experiment. In Figure 6, a sketch of the experimental setup is shown. The detection system consisted of two telescopes, each made of an ionization chamber (IC) and a position sensitive silicon detector (PSD), and two individual PSD detectors. Telescopes were optimized for ^{16}O detection, while PSDs were used to detect alpha particles. The angular position of the detectors were selected to maximize the QF contribution. Each PSD allows for the measurement of

both energy and impact position of the detected particles allowing for the measurement of the emission angle. Typical intrinsic resolution of a PSD is about 0.5% for energy and 300 μm for the position. The energy and angle of the third undetected particle, the neutron in the present case, were calculated by means of energy and momentum conservation laws. All the variables of interest were calculated from the energy and emission angle of the detected particles. These for example include the Q-value of the three-body as well as the Q-value and the center of mass energy of the two-body process. The acquisition of the event was triggered by the coincidence between the telescopes and any of the other two PSDs located on the other side of the beam axis.

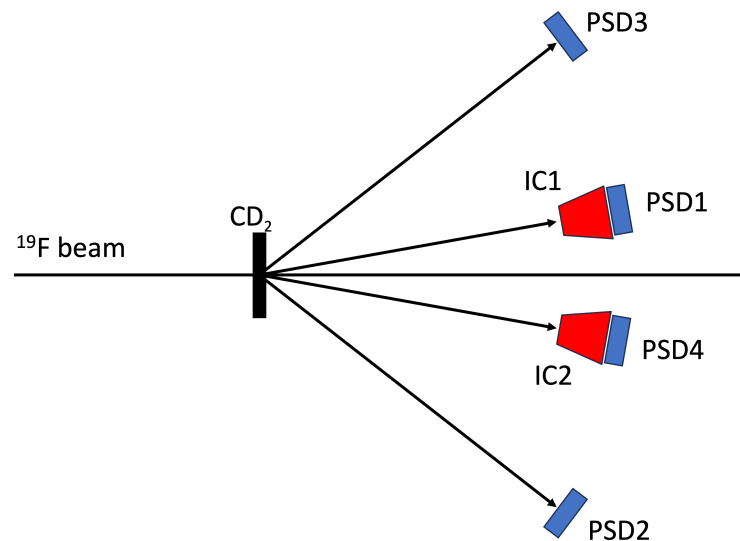


Figure 6. Sketch of the experimental setup.

3.1.2. Selection of the Reaction Channel and Mechanism

The selection of the reaction channel, that is ${}^2\text{H}({}^{19}\text{F},\alpha_0 {}^{16}\text{O})\text{n}$, was performed following the standard $\Delta\text{E-E}$ technique. Moreover, the Q-value of the three-body process has been evaluated and compared with the theoretical one for the ${}^2\text{H}({}^{19}\text{F},\alpha_0 {}^{16}\text{O})\text{n}$ channel (see Figure 7). Events belonging to the most prominent peak are selected for the following analysis. Further tests have been performed, such as the comparison between the experiment kinematical loci and that one obtained by a Monte Carlo simulation.

The applicability of THM and the cross-section factorization in PWIA are possible only if the reaction proceeds through a quasi-free breakup mechanism [27]. In order to verify the population of the reaction channel of interest by QF breakup mechanism, the momentum distribution of the neutron (spectator) is studied.

Following the procedure described in [43], the experimental momentum distribution has been extracted and compared with the theoretical one, which, for the deuteron, is given by the square of the Fourier transform of the Hulthén function.

The experimental distribution (black dots) and the theoretical one (red line) are shown in Figure 8. Within the experimental errors, a good agreement between the experimental data and the theoretical distribution is found. This result represents a strong experimental evidence of the population of the ${}^2\text{H}({}^{19}\text{F},\alpha_0 {}^{16}\text{O})\text{n}$ reaction by QF mechanism. Thus, events for neutron momentum $p_n < 30 \text{ MeV}/c$ were taken into account for the extraction of the ${}^{19}\text{F}(p,\alpha_0){}^{16}\text{O}$ two-body reaction S(E)-factor [44].

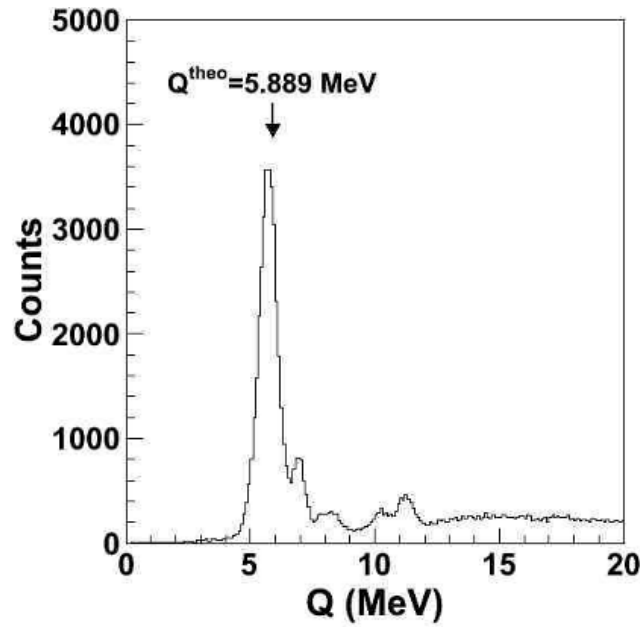


Figure 7. Experimental three-body Q-value. The main peak is due to the reaction channel of interest ${}^2\text{H}({}^{19}\text{F},\alpha){}^{16}\text{O}n$. The arrow indicates the theoretical value.

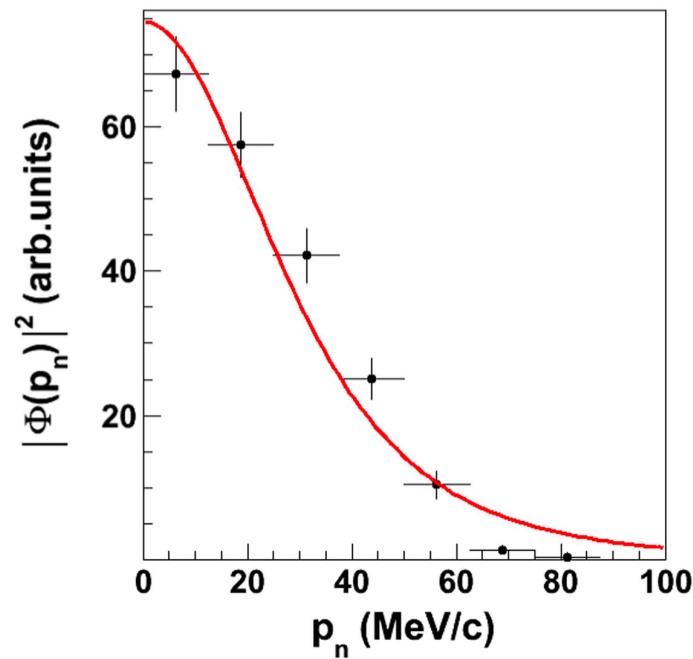


Figure 8. Experimental momentum distribution (full dots) compared with theoretical distribution, given by the square of the Hulthèn wave function in momentum space (red solid line) (adapted from [7]).

3.1.3. Extraction of the Astrophysical S(E)-Factor

According to the data selection described in the previous paragraphs, in Figure 9, the QF three-body coincidence yield as a function of the center of mass energy of the two-body process $E_{c.m.}$ is shown. This energy is given by the following equation:

$$E_{c.m.} = E_{16\text{O}-\alpha} - Q_2 \tag{3}$$

where $E_{16\text{O}-\alpha}$ is the ${}^{16}\text{O} - \alpha$ relative energy and Q_2 is the Q-value of the ${}^{19}\text{F}(p,\alpha){}^{16}\text{O}$ process.

The experimental data are characterized by several resonances due to the population of ^{20}Ne excited levels. In Table 1, the ^{20}Ne resonances considered in the THM data analysis are listed.

It is worth noting that the resonances inside the energy range of astrophysical interest ($E_{c.m.} \leq 300$ keV), at energies 113 keV and 251 keV, have been observed for the first time, allowing for the evaluation of their astrophysical impact [6,7]. The only direct measurement that reached the high energy tail of the astrophysical region was provided in [19] ($E_{c.m.} = 0.2\text{--}0.6$ MeV), where the smooth increase of astrophysical factor and the analysis of the angular distributions suggests the possible existence of resonances at $E_{c.m.} < 300$ keV.

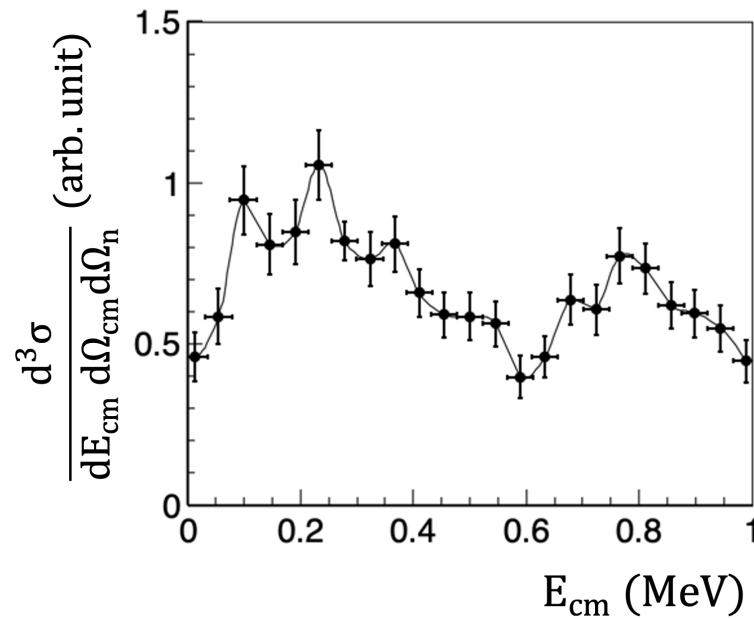


Figure 9. THM triple differential cross-section of the $^{19}\text{F}(p,\alpha_0)^{16}\text{O}$ reaction. The vertical error bars consider the statistical uncertainty only. The horizontal error bars are due to the size of the integration bin. The black line interpolates experimental data [7].

Table 1. ^{20}Ne resonances considered in the THM data analysis.

E^* (MeV)	J^π	$E_{c.m.}$ keV
12.957	2^+	113
13.095	2^+	251
13.222 ^a	0^+	
13.224 ^a	1^-	380
13.226 ^a	3^+	
13.529 ^a	2^+	696
13.586 ^a	2^+	739
13.642	2^+	798

^a unresolved peaks.

Following the procedure described in [7] the contribution of each resonance was disentangled using a multi-Gaussian fit. Then, angular distribution of each resonance was evaluated to obtain the THM angular integrated cross-section. Since THM does not provide the cross-section in absolute value, THM data have to be normalized to direct measurements. This was performed considering the energy region above 600 keV where THM data overlaps with direct measurement [20]. The non-resonant background contribution was considered as in [19].

In order to extract the reduced widths of the populated resonances, THM data were fitted with Equation (2). Given that the same reduced widths are present in both modi-

fied and standard R-matrix equations, the resonance parameters obtained by fitting the experimental THM cross-section were subsequently considered in the standard R-matrix calculation. This enabled us to obtain the astrophysical $S(E)$ -factor for the $^{19}\text{F}(p,\alpha_0)^{16}\text{O}$ reaction at low energies of astrophysical interest. More details on the analysis procedure are provided in [6,7].

4. Direct Data and THM Data: Comparison

In Figure 10, the astrophysical $S(E)$ -factors measured with the two described experimental approaches are shown. In particular, black dots represent the THM $S(E)$ -factor where the error bars are due to the combined statistical and systematic error (see [7] for more details). The direct data are reported with red dots and corresponding error bars that account for 0.5% in the horizontal axis, while the vertical bars display the total error equal to 12–15%. A detailed description of the uncertainty sources can be found in [25]. These data sets exhibit a trend well in agreement with the recent data published in [19] and can be used to normalize the THM data, demonstrating an excellent agreement between the two approaches.

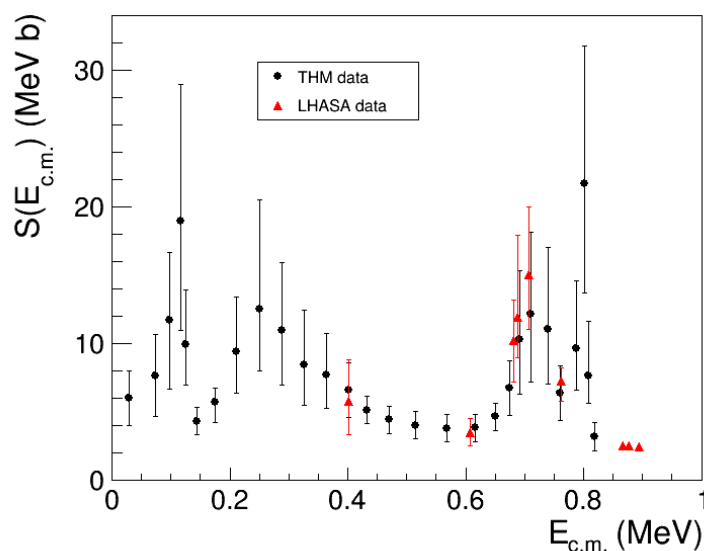


Figure 10. Comparison between the THM data (black dots [7]) and the direct data obtained with the LHASA detector (red dots [25]). The excellent agreement is a clear demonstration of the consistency and solidity of the direct and indirect approaches.

As previously stated, the error bar affecting the α_0 reaction rate cannot be directly transferred to the total reaction rate, an unknown fraction of the total cross-section being unconstrained. Specifically, the $^{19}\text{F}(p,\alpha_\pi)^{16}\text{O}$ experimental data stops at about 600 keV, as reported in Figure 11, where experimental data from [17,18,45,46] are reported. Below 0.6 MeV, only a non-resonant contribution is still considered in the astrophysical models, making those calculations only a lower limit for the real reaction rate. An R-matrix fit of the available experimental data provided by [47] (red line in Figure 11) shows an increase in the $S(E)$ -factor in an energy range of astrophysical interest if a resonant contribution due to the 13.095 MeV state of ^{20}Na is considered. In this framework, new measurements of the α_π are required to investigate possible resonant contribution at low energies.

In the following, we present an overview of the experimental campaign performed by the AsFiN collaboration in order to shed light on the α_π channel contribution for the total astrophysical $S(E)$ -factor of the $^{19}\text{F}(p,\alpha)^{16}\text{O}$ reaction. Indeed, taking advantage of the good results obtained with direct and indirect measurement for the α_0 channel, we conducted two experiments focused on the measurement of the $^{19}\text{F}(p,\alpha_\pi)^{16}\text{O}$ reaction cross-section.

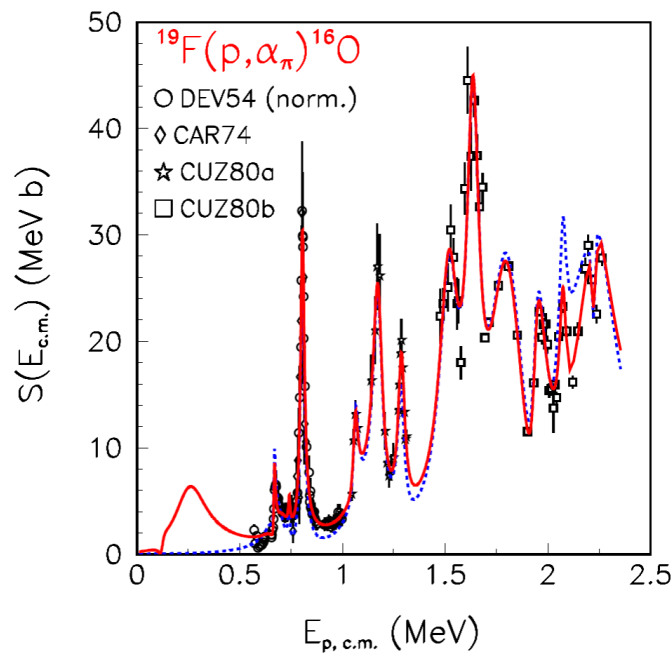


Figure 11. $S(E)$ -factor of the $^{19}\text{F}(p, \alpha_{\pi})^{16}\text{O}$ reaction as a function of the center-of-mass energy. Experimental data are from [17] (open diamonds), [18] (open stars), [45] (open circles) and [46] (open squares). The red solid line represents the result an R-matrix fit of data, considering the contribution of the 13.095 MeV state of ^{20}Na . Dashed blue line represents the R-matrix fit without the contribution of the mentioned ^{20}Na state [47].

4.1. Direct Approach: LHASA + ELISSA Detectors

Due to the very small energy separation between the (p, α_{π}) and (p, α_{γ}) channel of interest (<100 keV), good energy resolution is a crucial parameter for the measurement. In order to check the possibility to resolve and identify the different channels of the reaction, a preliminary study was performed with the GROOT simulation code [23]. The results of the simulation are reported in Figure 12, for the beam energy of 15 MeV, where it is possible to recognize the target reaction, the $^{19}\text{F}(p, \alpha)^{16}\text{O}$ with the three open channels (p, α_0) , (p, α_{π}) and (p, α_{γ}) , and also two other reactions coming from the carbon in the target, the $^{19}\text{F}(^{12}\text{C}, \alpha)^{27}\text{Al}$ and the $^{19}\text{F}(^{12}\text{C}, d)^{29}\text{Si}$ reactions. The carbon scattering due to the fluorine beam is also shown, while the scattered protons have a maximum energy of 3 MeV and are not displayed in the picture for clarity. The simulation takes into account the energy and position resolution considering beam energy spread, target thickness and detector resolution and clearly demonstrate the possibility of our setup to distinguish between the different expected channels.

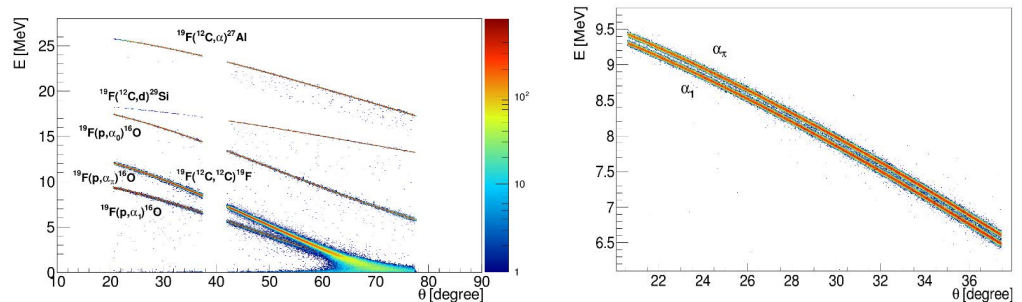


Figure 12. Monte Carlo simulation for the expected reaction channels. See text for details.

The experiment was performed at IFIN-HH, Magurele (Romania), the 3 MV Tandatron accelerator provided the ^{19}F beam with an energy range from 7 to 15 MeV with a diameter of the spot size on target of 1 mm and intensities around 1–5 nA. Thin self-supported

polyethylene targets (CH_2) of about $50 \mu\text{g}/\text{cm}^2$ were placed at 90° with respect to the beam direction and were frequently changed to avoid degradation. The thickness of the target guaranteed a good energy and position resolution reducing as much as possible the energy spread due to the straggling. The emerging α particles were detected by the LHASA array coupled with the ELISSA (Extreme Light Infrastructure Silicon Strip Array) [48,49] detector system, which was able to measure energy and angle of emission with high precision. Indeed, the ELISSA detector array used for this experiment consists of one ring of 12 X3 position sensitive silicon strip detectors with four front strips [21] that secure an excellent kinematical identification of the induced reactions. The detection system used, shown in Figure 13, ensured a wide angular coverage (from 8° to 50°) and was placed at 5 cm from the target. The calibration procedure consisted of mounting equally spaced grids in front of the X3 detectors to perform the position calibration and using a thorium alpha source for energy calibration below 4 MeV, while for energy calibration up to 20 MeV a ^6Li beam at different energies impinging on a gold target was used. The analysis of the experimental data is still in progress.

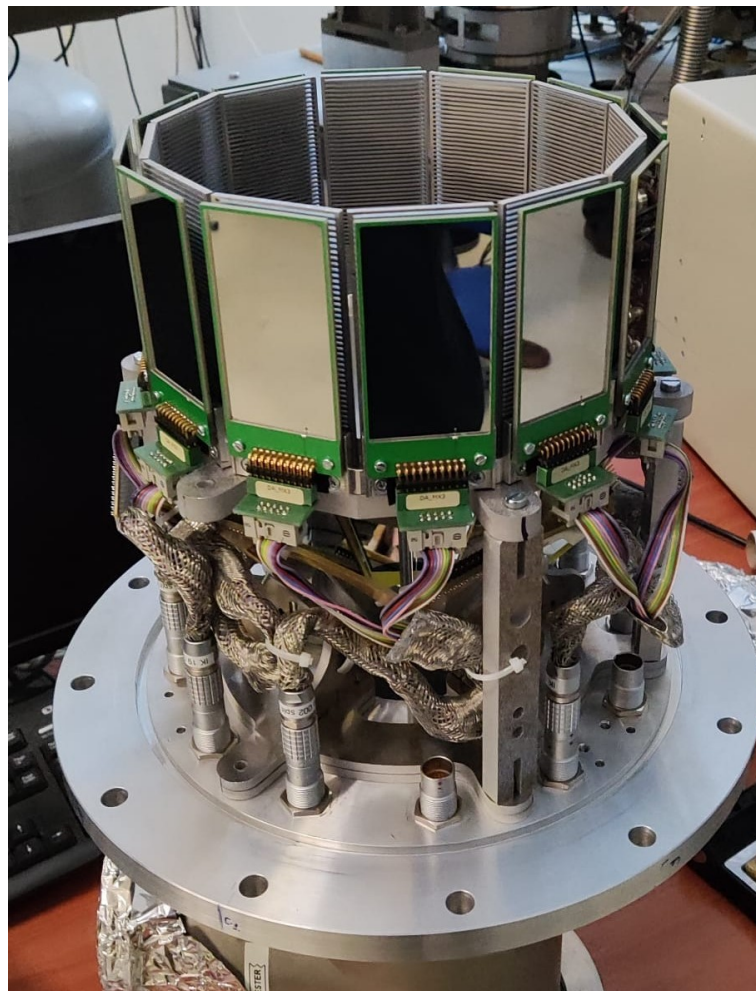


Figure 13. Picture of the experimental setup used for the experiment. A scaled version of the full ELISSA array (one ring on top) was coupled with the LHASA array (down in the picture).

4.2. Indirect Approach via THM

The study of the $^{19}\text{F}(p,\alpha\pi)^{16}\text{O}$ reaction has been tackled also applying the THM. The experiment has been performed at LNS-INFN, where the Tandem accelerator provided a 55 MeV ^{19}F beam delivered on a CD_2 target, $100 \mu\text{g}/\text{cm}^2$ thick. The detection setup was very similar to that one used for the (p,α_0) channel. Two telescopes made of an IC plus a $1000 \mu\text{m}$ PSD were placed at forward angles and symmetrically with respect to the

beamline. Four more PSDs were positioned at larger angles, two on each side of the beam line. ICs have been optimized for ^{16}O detection, while PSDs were optimized for α particles. Detectors were placed in order to cover the QF kinematical region. The experiment will allow us to extract the astrophysical $S(E)$ -factor in a wide energy range, down to zero energy, covering the astrophysical energy region where currently only a non-resonant extrapolation is considered [8], but where the contribution of a resonance is expected [47] (see Figure 11). The experiment will also allow the study of the $(p,\alpha\gamma)$ channel and to investigate the contribution of a possible resonance at 11 keV, as recently highlighted in [10]. Data analysis is ongoing.

5. Conclusions

In an attempt to solve the discrepancy between the available data in the literature for the $^{19}\text{F}(p,\alpha_0)^{16}\text{O}$ and the lack of data reported in the NACRE compilation for the $^{19}\text{F}(p,\alpha_\pi)^{16}\text{O}$ reaction cross-section, here, a new study was conducted by the AsFiN group with both direct approach using devoted detector arrays such as LHASA and ELISSA and indirect THM measurements. The presented results clearly show a new astrophysical $S(E)$ -factor for the (p,α_0) channel, covering the energy region of interest for stellar evolution models, while the on the base of the good results obtained, a new campaign of both direct and THM measurements have been performed to study the α_π channel at low energies, down to the astrophysical energy region, making us confident to provide a comprehensive evaluation of the $^{19}\text{F}(p,\alpha)^{16}\text{O}$ reaction rate and its astrophysical impact, with particular reference to the ratio $(p,\gamma)/(p,\alpha)$ between the two fluorine destruction channels.

Author Contributions: Methodology, G.L.G. and G.G.R.; Formal analysis, G.L.G., G.G.R. and T.P.; Data curation, G.L.G., G.G.R., M.L.C. (Marco La Cognata), T.P., X.S. and N.V.; Writing—original draft, G.L.G. and G.G.R.; Writing—review & editing, D.L.B., G.D.A., A.D.P., P.F., M.L.C. (Marco La Cognata), M.L.C. (Marco La Commara), L.L., D.L., C.M., M.M., A.A.O., S.P., T.P., R.G.P., S.R., M.L.S., R.S., X.S., A.T. and N.V.; Project administration, G.G.R.; Funding acquisition, D.L.B. and C.M. All authors have read and agreed to the published version of the manuscript.

Funding: This work was partially supported by the Extreme Light Infrastructure Nuclear Physics Phase II, a project cofinanced by the Romanian Government and the European Union through the European Regional Development Fund—the Competitiveness Operational Programm (1/07.07.16, COP, ID1334), by ENSAR2, a project financed by the European Union’s Horizon 2020 research and innovation programm under grant agreement No. 654002, by the funds DGAPAUNAM IN107820 and CONACyT 315839 and by “PIAano di inCentivi per la Ricerca di Ateneo 2020/2022”—Linea di Intervento 3 STARTING GRANT 2020 of the University of Catania.

Data Availability Statement: All data generated during this study are contained in this published article.

Acknowledgments: The authors are grateful to acknowledge the support of the staff of the LNS/LNL/IFIN-HH technical division, LNS/LNL/IFIN-HH accelerator divisions and the LNS target laboratory for the continuous and helpful assistance.

Conflicts of Interest: The authors declare no conflicts of interest.

References

1. Cristallo, S.; Straniero, O.; Gallino, R.; Piersanti, L.; Domínguez, I.; Lederer, M.T. Evolution, nucleosynthesis and yields of low-mass Asymptotic Giant Branch stars at different metallicities. *Astrophys. J.* **2009**, *696*, 797. [[CrossRef](#)]
2. Jonsson, H.; Ryde, N.; Spitoni, E.; Matteucci, F.; Cunha, K.; Smith, V.; Hinkle, K.; Schultheis, M. Fluorine in the solar neighborhood: No evidence for the neutrino process. *Astrophys. J.* **2017**, *835*, 50. [[CrossRef](#)]
3. Abia, C.; Cunha, K.; Cristallo, S.; Laverny, P. The origin of fluorine: Abundances in AGB carbon stars revisited. *A&A* **2015**, *581*, A88.
4. Lugaro, M.; Ugalde, C.; Karakas, A.I.; Gorres, J.; Wiescher, M.; Lattanzio, J.C.; Cannon, R.C. Reaction Rate Uncertainties and the Production of ^{19}F in Asymptotic Giant Branch Stars. *Astrophys. J.* **2004**, *615*, 934. [[CrossRef](#)]
5. Palmerini, S.; D’Agata, G.; La Cognata, M.; Indelicato, I.; Pizzone, R.G.; Trippella, O.; Vescovi, D. $^{19}\text{F}(p,\alpha)^{16}\text{O}$ and $^{19}\text{F}(\alpha,p)^{22}\text{Ne}$ Reaction Rate Measured via THM and Fluorine Nucleosynthesis in AGB stars. *J. Phys. Conf. Ser.* **2019**, *1308*, 012016. [[CrossRef](#)]

6. La Cognata, M.; Mukhamedzhanov, A.M.; Spitaleri, C.; Indelicato, I.; Aliotta, M.; Burjan, V.; Cherubini, S.; Coc, A.; Gulino, M.; Hons, Z.; et al. The fluorine destruction in stars: First experimental study of the $^{19}\text{F}(p,\alpha_0)^{16}\text{O}$ reaction at astrophysical energies. *Astrophys. J. Lett.* **2011**, *739*, L54. [[CrossRef](#)]
7. Indelicato, I.; La Cognata, M.; Spitaleri, C.; Burjan, V.; Cherubini, S.; Gulino, M.; Hayakawa, S.; Hons, Z.; Kroha, V.; Lamia, L.; et al. New Improved Indirect Measurement of the $^{19}\text{F}(p,\alpha)^{16}\text{O}$ Reaction at Energies of Astrophysical Relevance. *Astrophys. J.* **2017**, *19*, 845. [[CrossRef](#)]
8. Angulo, C.; Arnould, M.; Rayet, M.; Descouvemont, P.; Baye, D.; Leclercq-Willain, C.; Coc, A.; Barhoumi, S.; Aguer, P.; Rolfs, C.; et al. A compilation of charged-particle induced thermonuclear reaction rates. *Nucl. Phys. A* **1999**, *656*, 3. [[CrossRef](#)]
9. Clarkson, O.; Herwig, F. Convective H-He interactions in massive population III stellar evolution models. *Mon. Not. R. Astron. Soc.* **2021**, *500*, 2685–2703. [[CrossRef](#)]
10. Zhang, L.Y.; Su, J.; He, J.J.; Wiescher, M.; deBoer, R.J.; Kahl, D.; Chen, Y.J.; Li, X.Y.; Wang, J.G.; Zhang, L.; et al. Direct Measurement of the Astrophysical $^{19}\text{F}(p,\alpha_\gamma)^{16}\text{O}$ Reaction in the Deepest Operational Underground Laboratory. *Phys. Rev. Lett.* **2021**, *127*, 152702. [[CrossRef](#)]
11. Zhang, L.Y.; He, J.; deBoer, R.J.; Wiescher, M.; Heger, A.; Kahl, D.; Su, J.; Odell, D.; Chen, Y.; Li, X.; et al. Measurement of $^{19}\text{F}(p,\gamma)^{20}\text{Ne}$ reaction suggests CNO breakout in first stars. *Nature* **2022**, *610*, 656. [[CrossRef](#)] [[PubMed](#)]
12. Wiescher, M.; Görres, J.; Schatz, H. Break-out reactions from the CNO cycles. *J. Phys. G Nucl. Part. Phys.* **1999**, *25*, R133. [[CrossRef](#)]
13. Abia, C.; Recio-Blanco, A.; de Laverny, P.; Cristallo, S.; Domínguez, I.; Straniero, O. Fluorine in AGB Carbon Stars Revisited. *Astrophys. J.* **2009**, *694*, 971. [[CrossRef](#)]
14. Abia, C.; Cunha, K.; Cristallo, S.; de Laverny, P.; Domínguez, I.; Eriksson, K.; Gialanella, L.; Hinkle, K.; Imbriani, G.; Recio-Blanco, A.; et al. Fluorine abundances in galactic Asymptotic Giant Branch stars. *Astrophys. J.* **2010**, *715*, L94. [[CrossRef](#)]
15. Breuer, G. Messung und Analyse von Winkelverteilung und Wirkungsquerschnitt der Reaktion $\text{F}^{19}(p,\alpha_0)\text{O}^{16}$ im Energiebereich 0,4 bis 0,72 MeV. *Z. Phys.* **1959**, *154*, 339. [[CrossRef](#)]
16. Isoya, A. Analysis of the yield curves and the angular distributions of the reactions $\text{F}^{19}(p,\alpha_0)\text{O}^{16}$ and $\text{F}^{19}(p,\alpha_\pi)\text{O}^{16}$. *Nucl. Phys. A* **1959**, *7*, 126. [[CrossRef](#)]
17. Caracciolo, R.; Cuzzocrea, P.; DeRosa, A.; Inghima, G.; Perillo, E.; Sandoli, M.; Spadaccini, G. The 13.645 MeV state in ^{20}Ne . *Lett. Nuovo Cimento* **1974**, *11*, 33. [[CrossRef](#)]
18. Cuzzocrea, P.; De Rosa, A.; Inghima, G.; Perillo, E.; Rosato, E.; Sandoli, M.; Spadaccini, G. Quartet states in ^{20}Ne . *Lett. Nuovo Cimento* **1980**, *28*, 515. [[CrossRef](#)]
19. Lombardo, I.; Dell'Aquila, D.; Di Leva, A.; Indelicato, I.; La Cognata, M.; La Commara, M.; Ordine, A.; Rigato, V.; Romoli, M.; Rosato, M.; et al. Toward a reassessment of the $^{19}\text{F}(p,\alpha_0)^{16}\text{O}$ reaction rate at astrophysical temperatures. *Phys. Lett. B* **2015**, *748*, 178. [[CrossRef](#)]
20. Lombardo, I.; Dell'Aquila, D.; Campajola, L.; Rosato, E.; Spadaccini, G.; Vigilante, M. Analysis of the $^{19}\text{F}(p,\alpha_0)^{16}\text{O}$ reaction at low energies and the spectroscopy of ^{20}Ne . *J. Phys. G Nucl. Part. Phys.* **2013**, *40*, 125102. [[CrossRef](#)]
21. Micron Semiconductor, General Catalogue. Available online: <https://www.micronsemiconductor.co.uk/silicon-detector-catalogue/> (accessed on 14 July 2024).
22. Guardo, G.L.; Lattuada, D.; Petrusse, T. Developing system arrays for new experimental approach in nuclear astrophysics. *J. Phys. Conf. Ser.* **2023**, *2619*, 012009. [[CrossRef](#)]
23. Lattuada, D.; Balabanski, D.L.; Chesnevskaya, S.; Costa, M.; Crucillà, V.; Guardo, G.L.; La Cognata, M.; Matei, C.; Pizzone, R.G.; Romano, S.; et al. A fast and complete GEANT4 and ROOT Object-Oriented Toolkit: GROOT. *EPJ Web Conf.* **2017**, *165*, 01034. [[CrossRef](#)]
24. Brun, R.; Rademakers, F. ROOT: An object oriented data analysis framework. *Nucl. Instrum. Methods Phys. Res. Sect. A Accel. Spectrom. Detect. Assoc. Equip.* **1997**, *389*, 81. [[CrossRef](#)]
25. Guardo, G.L.; Petrusse, T.; Lattuada, D.; La Cognata, M.; Balabanski, D.L.; Açıköz, E.; Acosta, L.; Capponi, L.; Carbone, D.; Cherubini, S.; et al. Direct measurement of the $^{19}\text{F}(p,\alpha_0)^{16}\text{O}$ reaction at $E = 0.4\text{--}0.9$ MeV using the LHASA detector array. *Eur. Phys. J. A* **2023**, *59*, 65. [[CrossRef](#)]
26. Petrusse, T.; Guardo, G.L.; Lattuada, D.; La Cognata, M.; Balabanski, D.L.; Açıköz, E.; Acosta, L.; Capponi, L.; Carbone, D.; Cherubini, S.; et al. Submitted to EPJ, tag number EPJA-107832, Under Review.
27. Spitaleri, C.; La Cognata, M.; Lamia, L.; Pizzone, R.G.; Tumino, A. Astrophysics studies with the Trojan Horse Method. *Eur. Phys. J. A* **2019**, *55*, 161. [[CrossRef](#)]
28. Pizzone, R.G.; Bertulani, C.A.; Lamia, L.; La Cognata, M.; Sergi, M.L.; Spartá, R.; Tumino, A. Clusters and their fundamental role for Trojan Horse Method. *Eur. Phys. J. A* **2020**, *56*, 283. [[CrossRef](#)]
29. Tumino, A.; Bertulani, C.A.; La Cognata, M.; Lamia, L.; Pizzone, R.G.; Romano, S.; Typel, S. The Trojan Horse Method: A Nuclear Physics Tool for Astrophysics. *Annu. Rev. Nucl. Part. Sci.* **2021**, *71*, 345–376. [[CrossRef](#)]
30. Tribble, R.E.; Bertulani, C.A.; Mukhamedzhanov, A.M.; Spitaleri, C. Indirect techniques in nuclear astrophysics: A review. *Rep. Prog. Phys.* **2014**, *77*, 106901. [[CrossRef](#)] [[PubMed](#)]
31. Mukhamedzhanov, A.M.; Blokhintsev, L.D.; Irgaziev, B.F.; Kadyrov, A.S.; La Cognata, M.; Spitaleri, C.; Tribble, R.E. Trojan Horse as an indirect technique in nuclear astrophysics. *J. Phys. G Nucl. Part. Phys.* **2008**, *35*, 014016. [[CrossRef](#)]

32. Rapisarda, G.G.; Spitaleri, C.; Cvetinović, A.; Spartà, R.; Cherubini, S.; Guardo, G.L.; Gulino, M.; La Cognata, M.; Lamia, L.; Pizzone, R.G.; et al. Study of the $10\text{B}(p,\alpha_1)^7\text{Be}$ reaction by means of the Trojan Horse Method. *Eur. Phys. J. A* **2018**, *54*, 189. [[CrossRef](#)]
33. Cvetinovic, A.; Spitaleri, C.; Spartà, R.; Rapisarda, G.G.; Puglia, S.M.R.; La Cognata, M.; Cherubini, S.; Guardo, G.L.; Gulino, M.; Lamia, L.; et al. Trojan horse measurement of the $10\text{B}(p,\alpha_0)^7\text{Be}$ cross section in the energy range from 3 keV to 2.2 MeV. *Phys. Rev. C* **2018**, *97*, 065801. [[CrossRef](#)]
34. Palmerini, S.; La Cognata, M.; Hammache, F.; Acosta, L.; Alba, R.; Burjan, V.; Chávez, E.; Cherubini, S.; Cvetinović, A.; D'Agata, G.; et al. The $27\text{Al}(p,\alpha)^{24}\text{Mg}$ reaction at astrophysical energies studied by means of the Trojan Horse Method applied to the $2\text{H}(27\text{Al},\alpha^{24}\text{Mg})\text{n}$ reaction. *Eur. Phys. J. Plus* **2021**, *136*, 898. [[CrossRef](#)]
35. La Cognata, M.; Palmerini, S.; Adsley, P.; Hammache, F.; Di Pietro, A.; Figuera, P.; Dell'Agli, F.; Alba, R.; Cherubini, S.; Guardo, G.L.; et al. A New Reaction Rate of the $27\text{Al}(p,\alpha)^{24}\text{Mg}$ Reaction Based on Indirect Measurements at Astrophysical Energies and Implications for 27Al Yields of Intermediate-mass Stars. *Astrophys. J.* **2022**, *941*, 96. [[CrossRef](#)]
36. Guardo, G.L.; Spitaleri, C.; Lamia, L.; Spartà, R.; Carlin, N.; Cherubini, S.; Del Santo, G.; Indelicato, I.; La Cognata, M.; Lattuada, D.; et al. The $10\text{B}(n,\alpha)^7\text{Li}$ cross sections at ultra-low energy through the Trojan Horse Method applied to the $2\text{H}(10\text{B},\alpha^7\text{Li})^1\text{H}$. *Eur. Phys. J. A* **2019**, *55*, 211. [[CrossRef](#)]
37. Pizzone, R.G.; Spampinato, C.; Spartà, R.; Couder, M.; Tan, W.; Burjan, V.; D'Agata, G.; Guardo, G.L.; La Cognata, M.; Lamia, L.; et al. Indirect measurement of the $3\text{He}(n,p)^3\text{H}$ reaction cross section at Big Bang energies. *Eur. Phys. J. A* **2020**, *56*, 199. [[CrossRef](#)]
38. Spartà, R.; Lamia, L.; La Cognata, M.; Spitaleri, C.; Rapisarda, G.G.; Guardo, G.L.; Cherubini, S.; D'Agata, G.; Di Pietro, A.; Figuera, P.; et al. $10\text{B}(n,\alpha_0)^7\text{Li}$ and $10\text{B}(n,\alpha_1)^7\text{Li}$ reactions measured via Trojan Horse Method. *Eur. Phys. J. A* **2021**, *57*, 170.
39. Spartà, R.; Pizzone, R.G.; Bertulani, C.A.; Hou, S.; Lamia, L.; Tumino, A. Direct and Indirect Measurements for a Better Understanding of the Primordial Nucleosynthesis. *Front. Astron. Space Sci.* **2020**, *7*, 560149. [[CrossRef](#)]
40. Rapisarda, G.G.; Lamia, L.; Caciolli, A.; Chengbo, L.; Degl'Innocenti, S.; Depalo, R.; Palmerini, S.; Pizzone, R.G.; Romano, S.; Spitaleri, C.; et al. Experimental Nuclear Astrophysics With the Light Elements Li, Be and B: A Review. *Front. Astron. Space Sci.* **2021**, *7*, 589240. [[CrossRef](#)]
41. Sergi, M.L.; D'Agata, G.; Guardo, G.L.; Rapisarda, G.G.; Burjan, V.; Cherubini, S.; Gulino, M.; Indelicato, I.; La Cognata, M.; Lamia, L.; et al. Trojan Horse Investigation for AGB Stellar Nucleosynthesis. *Universe* **2022**, *8*, 128. [[CrossRef](#)]
42. Spartà, R.; La Cognata, M.; Guardo, G.L.; Palmerini, S.; Sergi, M.L.; D'Agata, G.; Lamia, L.; Lattuada, D.; Oliva, A.A.; Pizzone, R.G.; et al. Neutron-Driven Nucleosynthesis in Stellar Plasma. *Front. Phys.* **2022**, *10*, 896011. [[CrossRef](#)]
43. Lamia, L.; La Cognata, M.; Spitaleri, C.; Irgaziev, B.; Pizzone, R.G. Influence of the d-state component of the deuteron wave function on the application of the Trojan horse method. *Phys. Rev. C* **2012**, *85*, 025805. [[CrossRef](#)]
44. Shapiro, I.S. *Interaction of High-Energy Particles with Nuclei*; Academic: New York, NY, USA, 1967; p. 210
45. Devons, S.; Goldring, G. Emission of Electron-Positron Pairs from Light Nuclei II: γ -Transitions in 8Be , 10B and 16O . *Proc. Phys. Soc. A* **1954**, *67*, 413. [[CrossRef](#)]
46. Cuzzocrea, P.; De Rosa, A.; Inghima, G.; Perillo, E.; Rosato, E.; Sandoli, M.; Spadaccini, G. The $19\text{F}(p,\alpha)^{16}\text{O}$ Reaction and the Quartet Model. INFN Report INFN/BE-80/5. 1980. Available online: <https://www.inf.infn.it/sis/preprint/getfilepdf.php?filename=INFN-BE-80-5.pdf> (accessed on 14 July 2024).
47. Lombardo, I.; Dell'Aquila, D.; He, J.J.; Spadaccini, G.; Vigilante, M. New analysis of p+ 19F reactions at low energies and the spectroscopy of natural-parity states in 20Ne . *Phys. Rev. C* **2019**, *100*, 044307. [[CrossRef](#)]
48. Chesnevskaia, S.; Balabanski, D.L.; Choudhury, D.; Constantin, P.; Filipescu, D.M.; Ghita, D.G.; Guardo, G.L.; Lattuada, D.; Matei, M.; Rotaru, A.; et al. Performance studies of X3 silicon detectors for the future ELISSA array at ELI-NP. *J. Instrum.* **2018**, *13*, T05006. [[CrossRef](#)]
49. Guardo, G.L.; Anzalone, A.; Balabanski, D.L.; Chesnevskaia, S.; Crucillà, V.; Filipescu, D.; Gulino, M.; La Cognata, M.; Lattuada, D.; Matei, C.; et al. Development of the ELISSA array: Prototype testing at Laboratori Nazionali del Sud. *EPJ Web Conf.* **2018**, *184*, 02006. [[CrossRef](#)]

Disclaimer/Publisher's Note: The statements, opinions and data contained in all publications are solely those of the individual author(s) and contributor(s) and not of MDPI and/or the editor(s). MDPI and/or the editor(s) disclaim responsibility for any injury to people or property resulting from any ideas, methods, instructions or products referred to in the content.